IEEE Photonics Journal
An IEEE Photonics Society Publication

Measuring the Chirp and the Linewidth Enhancement Factor of Optoelectronic Devices with a Mach–Zehnder Interferometer

Volume 3, Number 3, June 2011

Jean-Guy Provost
Frederic Grillot, Member, IEEE

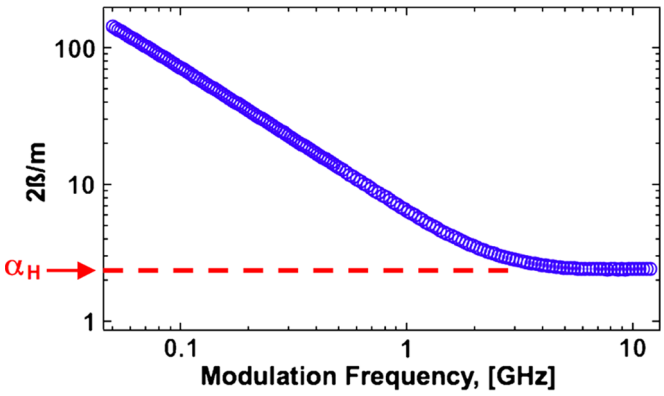

DOI: 10.1109/JPHOT.2011.2148194
1943-0655/$26.00 ©2011 IEEE

Measuring the Chirp and the Linewidth Enhancement Factor of Optoelectronic Devices with a Mach–Zehnder Interferometer

Jean-Guy Provost[1] **and Frederic Grillot,**[2,3] ***Member, IEEE***

[1]III-V Lab, a joint lab of Alcatel-Lucent Bell Labs France, Thales Research and Technology, and CEA Leti, 91460 Marcoussis, France
[2]Université Européenne de Bretagne, CNRS FOTON, Institut National des Sciences Appliquées, 35043 Rennes Cedex, France
[3]Institut TELECOM/Telecom Paristech, CNRS LTCI, 75634 Paris Cedex, France

DOI: 10.1109/JPHOT.2011.2148194
1943-0655/$26.00 ©2011 IEEE

Manuscript received April 20, 2011; accepted April 21, 2011. Date of publication April 29, 2011; date of current version May 20, 2011. Corresponding author: J.-G. Provost (e-mail: jean-guy.provost@3-5lab.fr).

Abstract: In this paper, a technique based on the use of a Mach–Zehnder (MZ) interferometer is proposed to evaluate chirp properties, as well as the linewidth enhancement factor (α_H-factor) of optoelectronic devices. When the device is modulated, this experimental setup allows the extraction of the component's response of amplitude modulation (AM) and frequency modulation (FM) that can be used to obtain the value of the α_H-factor. As compared with other techniques, the proposed method gives also the sign of the α_H-factor without requiring any fitting parameters and, thus, is a reliable tool, which can be used for the characterization of high-speed properties of semiconductor diode lasers and electroabsorption modulators. A comparison with the widely accepted fiber transfer function method is also performed with very good agreement.

Index Terms: Chirp, electroabsorption modulators, linewidth enhancement factor, optical modulation, semiconductor lasers.

1. Introduction

The linewidth enhancement factor (α_H-factor) is used to distinguish the behavior of semiconductor lasers (SLs) with respect to other types of lasers [1] and influences several fundamental aspects, such as the linewidth [1], [2], the chirp under modulation [3], the laser's behavior under optical feedback [4], [5], as well as the occurrence of the filamentation in broad-area lasers [6]. The α_H-factor is usually defined as the coupling between the phase and the amplitude of the electric field such as [1]

$$\alpha_H = -\frac{4\pi}{\lambda}\frac{dn/dN}{dg/dN} = -\frac{4\pi\Gamma}{\lambda}\frac{dn/dN}{dG_{net}/dN} \tag{1}$$

where λ is the lasing wavelength, N is the carrier density, g is the material gain, Γ is the optical confinement factor, and $G_{net} = \Gamma g - \alpha_i$ is the net modal gain with α_i the internal loss coefficient. The α_H-factor depends on the ratio of the evolution of the refractive index n with the carrier density N to that of the differential gain dg/dN. As reported in [7], several different techniques have been proposed to measure the α_H-factor, with no rigorous comparison between the results achieved, as

pointed out in [8]. Also, it should be stressed that the number of the proposed measuring methods has kept increasing while novel types of SLs, such as those based on quantum dot (QD), have arisen, for which the determination of the α_H-factor may be particularly critical [9].

In most cases, the α_H-factor is evaluated by using the so-called Hakki–Paoli subthreshold method, which relies on direct measurement of the refractive index change and the differential gain as the carrier density is varied by slightly changing the current of an SL [10], [11]. This method, which is applicable only below threshold, gives the material α_H-factor and does not correspond to an actual lasing condition. As a consequence of that, it makes more sense to determine the α_H-factor above the laser's threshold. Thus, relevant aspects such as the high-power behavior of the α_H-factor due to nonlinear effects and the consequences on the adiabatic chirp can be taken into account. Consequently, the α_H-factor appears as an optical power-dependent parameter that is strongly influenced by nonlinear gain and/or carrier heating effects [12]. Such a power-dependence is particularly strengthened in QD lasers in which the lasing wavelength can switch from the ground state (GS) to the excited state (ES) as the injected current increases. This accumulation of carrier in the ES arises, even though lasing in the GS that is still occurring enhances the effective α_H-factor of the GS transition introducing a nonlinear dependence with the injected current [9]. Among the above-threshold techniques used for extracting the α_H-factor, the linewidth method relies on the measurement of SL's linewidth, as well as on fitting the results to known SL's parameters [13]–[15]. Two other possibilities are based on injection-locking or on optical feedback techniques. On one hand, light from a master SL is injected into the slave SL, causing locking of the slave optical frequency to that of the master and an asymmetry in frequency due to the nonzero α_H-factor [16], [17]. On the other hand, the optical feedback method is based on the self-mixing interferometry configuration from which the α_H-factor is determined from the measurement of specific parameters of the resulting interferometric waveform [18]. Also, we can note that the α_H-factor of a distributed feedback (DFB) SL has been measured by using a phase-controlled high-resolution optical low-coherence reflectometer [19]. Finally, the determination of the α_H-factor can be conducted through high-frequency techniques. These methods are much more relevant when the performances of the device operating under direct modulation have to be evaluated for high-speed transmissions. On one hand, the SL current modulation generates both amplitude (AM) and optical frequency (FM) modulation [20]. The ratio of the FM over AM components gives a direct measurement of the α_H-factor [20]–[23]. The AM term can be measured by direct detection via a high-speed photodiode, while the FM term is related to sidebands intensity that can be measured using a high-resolution scanning Fabry–Perot filter. Although the FM/AM method requires modulation well above the SL's relaxation frequency, this technique gives the device α_H-factor under direct modulation. On the other hand, the fiber transfer function method originally proposed for the electroabsorption modulators (EAMs) [24] exploits the interaction between the chirp of a high-frequency modulated SL and the chromatic dispersion of an optical fiber, which produces a series of minima in the amplitude transfer function versus modulation frequency. Such a technique has then been generalized to diode lasers by introducing the adiabatic term, as shown in [25] and [26], and by fitting the measured transfer function, the α_H-factor can be retrieved. This method has been shown to be reliable, as long as precise measurement of fiber dispersion is made and as long as the power along the fiber span is kept enough low to avoid nonlinear effects. As compared with the FM/AM technique, the main disadvantage of such a method is that several fitting parameters have to be determined to access the α_H-factor.

Another important issue concerns the determination of the sign of the α_H-factor, which is of first importance for many applications requiring ultralow laser linewidth, such as on-chip pulse compression, chirp compensation, or for the EAMs. Among all the techniques explained above, only the fiber transfer function method can give the phase and then the sign of the α_H-factor. In this paper, an optical discriminator based on a tunable Mach–Zehnder (MZ) interferometer is used to extract AM and FM responses both in amplitude and in phase in the frequency domain as well as the α_H-factor. In Section 2, the basic equations needed to extract the α_H-factor, as well as the experimental setup, are presented. Section 3 shows experimental results on the α_H-factor of DFB lasers, EAMs, and integrated laser modulators (ILMs), as well as a comparison with measurements

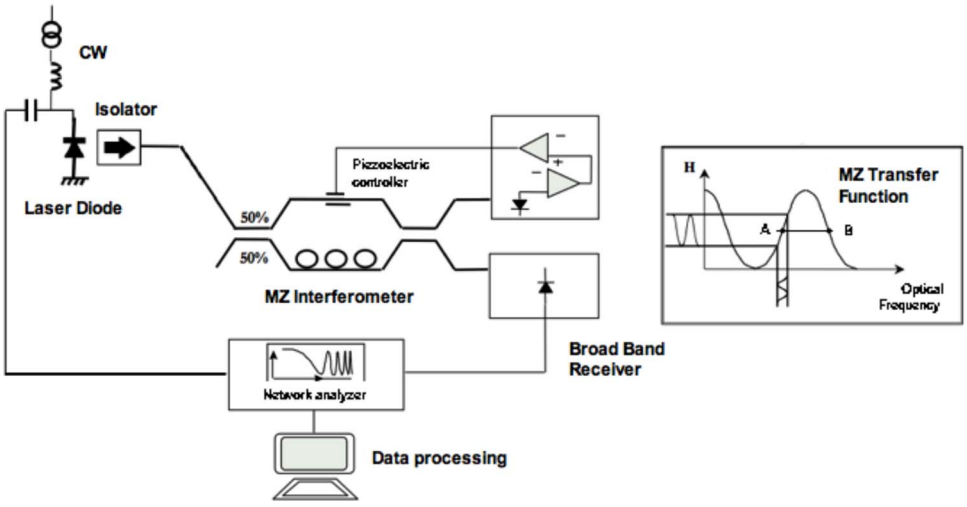

Fig. 1. Experimental setup used for the determination of AM, FM responses, and of the α_H-factor. (Inset) Transfer function of the interferometer.

obtained with the fiber transfer method. Finally, we summarize our results in Section 4. Although both Michelson and MZ interferometers have already been used in the past to measure the SL's FM responses [27]–[30], to the best of our knowledge, extractions of the chirp-to-power ratio (CPR) and of the α_H-factor have not been reported yet. As pointed out in [31], the FM and AM responses, as well as the α_H-factor, have been measured in the time domain through the MZ interferometer. Although such a technique remains very efficient when transient and adiabatic chirp contributions have to be separated [32], it does not lead to the same level of performances. Thus, because of the equipment limitations (PRBS generator with fixed transition time, sampling oscilloscope), the sensitivity, the dynamic, and the accuracy of the method is not as good as the one proposed in this paper. Let us stress that impact of the thermal effects is much more complicated to evaluate with large-signal measurements because low-frequency operation is required. Consequently, this interferometric technique is to be of first importance to measure the high-speed properties of the next generation of lasers and modulators.

2. Experimental Setup and Theory

2.1. Experimental Description

As depicted in Fig. 1, our experimental setup is similar to the one originally developed by Sorin *et al.* [33]. The goal is to determine the characteristics of the FM induced by the current modulation in the laser's cavity or the phase modulation (PM) for an external modulator. The signal at the output is analyzed through a tunable MZ interferometer made with two fibered couplers. This interferometer has a free-spectral range (FSR), which is the inverse of the differential delay $|T_2 - T_1|$ between the two arms, T_1 and T_2 being the propagation time (time delay) in the two arms, respectively. A polarization controller is used to make sure that the two signals located at the input of the second coupler have parallel states. The inset in Fig. 1 shows the power at the output of the interferometer as a function of the propagation time difference or of the optical frequency. To accurately control the optical path difference, a cylindrical piezoelectric transducer is used. The transducer located onto one of the MZ's arms is fiber interdependent and directly controlled by an external locking circuit. The system allows adjustment of the interferometer on all points of the characteristics. For instance, points A and B being in opposition, they correspond to two signals interfering in quadrature with each other, as shown in the inset of Fig. 1. Around these two locations, the interferometer's characteristics remaining linear, the photocurrent coming out from the

photodetector is proportional to the phase (or frequency) variations of the optical signal to be analyzed.

2.2. Theoretical Description of a Laser Under Direct Modulation (AM and FM)

The electric field from a laser under direct modulation can be expressed as follows:

$$e(t) = \sqrt{P_0}(1 + m\cos(2\pi f_m t))^{1/2} \times \exp j[2\pi f_0 t + \beta \sin(2\pi f_m t + \varphi)] \tag{2}$$

with P_0 the average power; m the modulation rate in power $(m = /P_0)$; f_m the frequency of the electrical signal provided by the network analyzer; f_0 the central optical frequency; β the modulation rate in frequency, such as $\beta \equiv \Delta F/f_m$ (ΔF being the amplitude of the FM across the optical carrier f_0); and φ the phase difference between the modulation frequency and the amplitude frequency. At the output of the interferometer, the signal can be written as

$$s(t) = \frac{1}{2}[e(t - T_1) + e(t - T_2)]. \tag{3}$$

By injecting (2) into (3)

$$\begin{aligned} s(t) = \frac{1}{2}\sqrt{P_0}[1 + m\cos(2\pi f_m(t - T_1))]^{1/2} \exp j[2\pi f_0(t - T_1) + \beta \sin(2\pi f_m(t - T_1) + \varphi] \\ + \frac{1}{2}\sqrt{P_0}[1 + m\cos(2\pi f_m(t - T_2))]^{1/2} \exp j[2\pi f_0(t - T_2) + \beta \sin(2\pi f_m(t - T_2) + \varphi]. \end{aligned} \tag{4}$$

As mentioned in Section 2.1., measurements are done at two different points A and B in opposition and corresponding to two signals interfering in quadrature with each other, meaning that $2\pi f_0(T_2 - T_1) = (\pi/2) + k\pi$, with k being an integer. Assuming this condition, the photocurrent going toward the network analyzer being proportional to $s(t)s^*(t)$ can be expressed as follows:

$$\begin{aligned} s(t)s^*(t) = \frac{P_0}{2}\left[1 + m\cos\left(\frac{\pi f_m}{FSR}\right)\cos\left(2\pi f_m\left(t - \frac{T_1 + T_2}{2}\right)\right)\right] \\ + \varepsilon\frac{P_0}{2}\left[1 + 2m\cos\left(\frac{\pi f_m}{FSR}\right)\cos\left(2\pi f_m\left(t - \frac{T_1 + T_2}{2}\right)\right)\right. \\ \left. + m^2\cos(2\pi f_m(t - T_1))\cos(2\pi f_m(t - T_2))\right]^{1/2} \\ \times \sin\left(2\beta\sin\left(\frac{\pi f_m}{FSR}\right)\cos\left(2\pi f_m\left(t - \frac{T_1 + T_2}{2}\right) + \varphi\right)\right). \end{aligned} \tag{5}$$

In (5), ε is a parameter whose value (± 1) depends on the position A or B, as depicted in the inset of Fig. 1, while $FSR = 1/|T_1 - T_2|$ is the FSR of the MZ interferometer. Also, it should be stressed that the network analyzer being sensitive only to the signal's components beating at the FM, all the continuous and higher order terms such as $(2f_m, 3f_m, \ldots)$ can be neglected [33]. Considering these assumptions, (5) can be rewritten as follows:

$$\begin{aligned} s(t)s^*(t) = \frac{P_0}{2}\left[m\cos\left(\frac{\pi f_m}{FSR}\right)\cos\left(2\pi f_m\left(t - \frac{T_1 + T_2}{2}\right)\right)\right] \\ + \varepsilon P_0 J_1\left(2\beta\sin\left(\frac{\pi f_m}{FSR}\right)\right)\cos\left(2\pi f_m\left(t - \frac{T_1 + T_2}{2}\right) + \varphi\right) \end{aligned} \tag{6}$$

with J_1 the Bessel function of the first kind, which can be approximated in most case such as $J_1(2\beta\sin(\pi f_m/FSR)) \approx \beta\sin(\pi f_m/FSR)$. As a consequence of that, (6) can be simplified and

rewritten such as

$$s(t)s^*(t)=\frac{P_0}{2}\left[m\cos\left(\frac{\pi f_m}{FSR}\right)\cos\left(2\pi f_m\left(t-\frac{T_1+T_2}{2}\right)\right)\right] + \varepsilon P_0\beta\sin\left(\frac{\pi f_m}{FSR}\right)\cos\left(2\pi f_m\left(t-\frac{T_1+T_2}{2}\right)+\varphi\right). \quad (7)$$

As shown in Fig. 1, the network analyzer giving two results associated with the A and B operating points, respectively, the normalized measured signals can be expressed as follows:

$$M_{\pm}=\frac{P_0}{2}m\cos\left(\frac{\pi f_m}{FSR}\right)\exp(-j2\pi f_m\tau)\pm P_0\beta\sin\left(\frac{\pi f_m}{FSR}\right)\exp j(-2\pi f_m\tau+\varphi) \quad (8)$$

where M_+ is the result in A and M_- in B, respectively, while $\tau=(T_1+T_2)/2$ is the transit time within the interferometer. On one hand, the first term in (8) only depends on the AM (i.e., β-independent), while the term $\cos(\pi f_m/FSR)$ corresponds to the AM transfer function of the interferometer [33]. On the other hand, the second term in (8) is purely related to the modulation frequency (m independent) and can be expressed as a function of the interferometer FM transfer function, such as $\pi P_0(\Delta F/FSR)\mathrm{sinc}(f_m/\ FSR)$ with $\mathrm{sinc}(x)=\sin(\pi x)/\pi x$.

From (8), following expressions can be deduced:

$$\frac{2\beta}{m}=\frac{1}{\tan\left(\frac{\pi f_m}{FSR}\right)}\left|\frac{M_+-M_-}{M_++M_-}\right| \quad (9a)$$

$$\varphi=\arg\left(\frac{M_+-M_-}{M_++M_-}\right). \quad (9b)$$

Using the definitions of parameters m and β, (9a) allows extraction of the CPR [34], such as

$$\frac{\Delta F}{\Delta P}=\frac{f_m}{2P_0}\frac{1}{\tan\left(\frac{\pi f_m}{FSR}\right)}\left|\frac{M_+-M_-}{M_++M_-}\right|. \quad (10)$$

The value of the α_H-factor is then determined through the so-called relationship [21]

$$\frac{2\beta}{m}=\alpha_H\sqrt{1+\left(\frac{f_c}{f_m}\right)^2}. \quad (11)$$

In (11), f_c is defined as the corner frequency [35]

$$f_c=\frac{1}{2\pi}v_g\frac{\partial g}{\partial P}P \quad (12)$$

with v_g the group velocity, P the output power, and $\partial g/\partial P$ a nonzero parameter because of the phenomenon of nonlinear gain related to nonzero intraband relaxation times, as well as carrier heating. Parameter $\partial g/\partial P$ can be expanded as a function of the gain compression factor ε_P following the relationship [36]:

$$\frac{\partial g}{\partial P}=\frac{\varepsilon_P g}{1+\varepsilon_P P}. \quad (13)$$

For typical numbers, the corner frequency can be in the hundreds of Megahertz to the few Gigahertz range, depending on the output power level. On one hand, for modulation frequencies such as $f_m \gg f_c$, which is the case in the experiment since the maximum modulation frequency f_m is

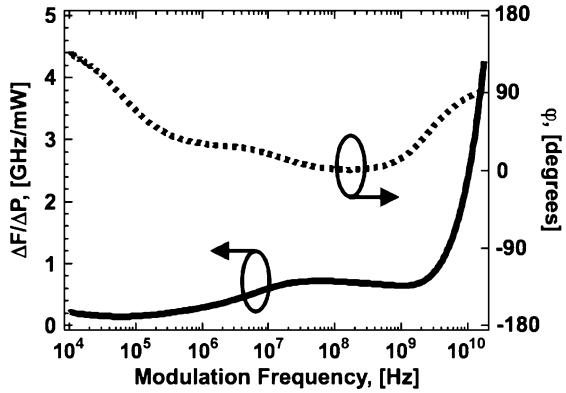

Fig. 2. Amplitude (solid line) and Phase (dotted line) of the CPR as a function of the modulation frequency for the QW DFB laser under study.

about in the 20-GHz range, the factor $2\beta/m$ directly equals the laser's α_H-factor. On the other hand, for lower modulation frequencies, the ratio $2\beta/m$ becomes inversely proportional to the modulation frequency. Let us note that the measurement of $2\beta/m$ with frequency and at different output power levels could serve for the determination of the corner frequency and, consequently, the gain compression factor.

2.3. Theoretical Description of an External Modulator (AM and PM)

In case of an external modulator the phase variation is given by [37]

$$\frac{d\phi(t)}{dt} = \frac{\alpha_H}{2}\frac{1}{P(t)}\frac{dP(t)}{dt} \tag{14}$$

with $\phi(t)$ the instantaneous phase of the optical signal and $P(t)$ the related power. Under a small signal analysis condition, the optical power $P(t)$ can be expressed such as

$$P(t) = P_0(1 + m\cos(2\pi f_m t)). \tag{15}$$

Then, it can be shown that the signal at the output of the modulator can be written following the relationship:

$$e(t) = \sqrt{P_0}(1 + m\cos(2\pi f_m t))^{1/2}\exp j\left(2\pi f_0 t + \frac{\alpha_H}{2} m\cos(2\pi f_m t)\right). \tag{16}$$

Based on a similar calculation as the one conducted in Section 2.2, the α_H-factor can be expressed as

$$\alpha_H = \frac{1}{j}\frac{1}{\tan\left(\frac{\pi f_m}{FSR}\right)}\left(\frac{M_+ - M_-}{M_+ + M_-}\right). \tag{17}$$

3. Experimental Results and Discussion

3.1. Case of a DFB Laser

The device under study is a DFB laser having a high reflection (HR) coating on the rear facet and an antireflection (AR) coating on the front facet to allow for high efficiency. The device is 350 μm long with an active layer made with quantum wells nanostructures. The threshold current is about 7.5 mA at room temperature (25 °C). In Fig. 2, the ratio $\Delta F/\Delta P$ in amplitude and in phase is depicted for a DFB laser operating under direct modulation in the range from 10 kHz to 15 GHz. The

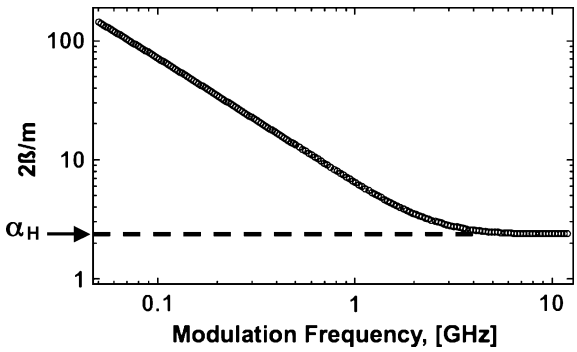

Fig. 3. $2\beta/m$ as a function of the modulation frequency for the QW DFB laser under study.

amplitude term of $\Delta F/\Delta P$ is obtained through (10), considering a 5-mW optical output power (this value is obtained for a DC bias current equal to 2.6 times the threshold current) for the laser under study, while the FSR equals 47.6 GHz (see the Appendix). With regard to the phase term of $\Delta F/\Delta P$, it is obtained from (9b). At low frequencies $(f_m < 10$ MHz$)$, thermal effects are predominant [3], [36]. When the modulation frequency decreases, the continuous wave regime gets closer, and the phase difference between the FM and AM responses tends to 180° [3], [36]. Such behavior is similar to the static operation case in which an increase in the laser's emitting wavelength (a decrease in the laser's optical frequency, respectively) is observed both with the injected current and with the output power. When 10 MHz $< f_m <$ 2 GHz, thermal effects are no longer significant, and the CPR is relatively constant. This regime corresponds to the adiabatic regime dominated by the gain compression effects and in which the AM and FM modulations are in-phase [3], [36]. Then, for larger frequencies $(f_m >$ 2 GHz$)$, relaxation oscillations between the carrier and photon numbers take place. The CPR gets proportional to f_m and the FM and AM responses are in quadrature with each other, leading to a 90° phase difference. In Fig. 3, the measured $2\beta/m$ ratio is plotted via (9a) starting from 50 MHz (beyond the thermal effects). As predicted by (11), the function $2\beta/m$ tends asymptotically to the α_H-factor, which is estimated to be about 2.4 for the laser under study.

3.2. Case of an EAM

In Fig. 4, the EAM's α_H-factor, as well as the corresponding phase, is evaluated through (17) for a monochromatic incident optical signal. On one hand, in Fig. 4(a), the α_H-factor is measured for a -2.0 V reverse voltage. This figure shows that the phase term remains constant and equal to zero so that the α_H-factor is positive ($+1.32$ in that case). On the other hand, Fig. 4(b) shows that when the reverse voltage decreases down to -3.2 V, the phase term drops to $-180°$ so that the measured α_H-factor gets negative (-1.20 in that case). Those results demonstrate that phase variations can be used to obtain the sign of the α_H-factor.

Let us note that for EAM-based devices, the α_H-factor remaining frequency-independent, measurements could be conducted at one frequency only, which is much quicker by comparison with the fiber transfer function method [24]. Indeed, to reach a good resolution on the minima of transmission, the fiber transfer method typically requires a wider span up to 15 or 20 GHz, as well as a lot of data points ($\sim$400). Considering the same component as well as the same wavelength, Fig. 5 shows a comparison between the two methods as a function of the bias voltage. As it can be shown, a very good agreement is demonstrated; in particular, the bifurcation point from which the α_H-factor switches from positive to negative values occurs at -2.6 V for both methods. However, when the bias voltage equals -4 V, which corresponds to $\alpha_H \sim -10$, the discrepancy between the two methods starts increasing. This discrepancy is due to the lower experimental accuracy which typically arises when the α_H-factors gets larger $(|\alpha_H| \geq 10)$, as pointed out in [24] for the fiber transfer function method and in Section 3.4 (see below) for the method under study.

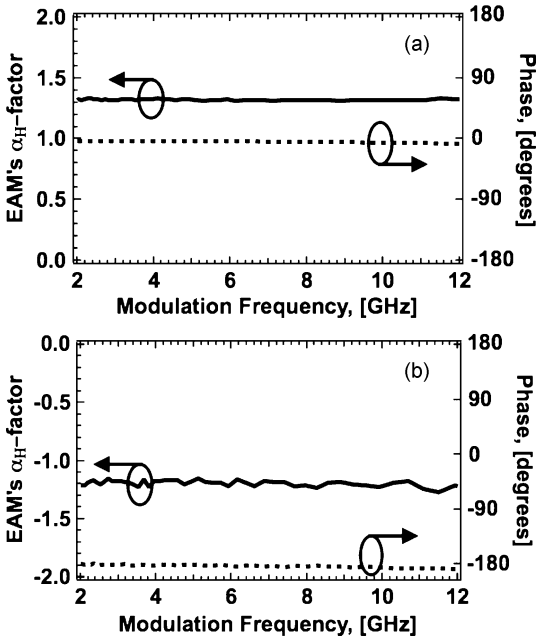

Fig. 4. Measured α_H-factor and phase as a function of the modulation frequency for the EAM. (a) V $= -2.0$ V. (b) V $= -3.2$ V.

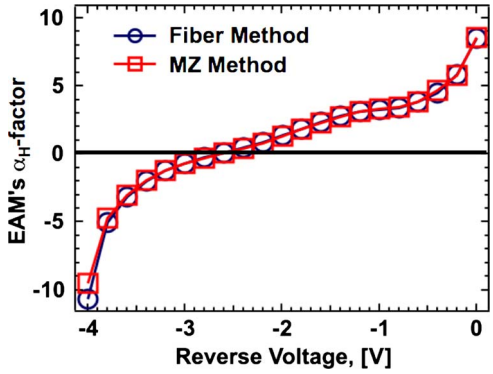

Fig. 5. Comparison of the α_H-factor measurements by the fiber method (blue line) and MZ method (red line) as a function of the reverse voltage for the EAM ($f_m = 10$ GHz).

3.3. Case of an ILM

Theoretically speaking, the chirp of an ILM should be similar to the one obtained for an isolated modulator, meaning that it should not be frequency-dependent, as already pointed out in Section 3.2. However, in an actual situation, a perturbation whose origin comes from an electrical or optical feedback is usually observed in the amplitude response [38], [39]. This unwanted feedback leads to either a positive or a negative dip arising close to the relaxation frequency of the laser section, as well as impacting the chirp behavior. Fig. 6(a) shows an example of the ILM's α_H-factor measured for a bias current of 100 mA (for the laser section) and for a -1 V bias voltage (for the EAM section). As shown, a dip occurring close to 7.7 GHz and with a full bandwidth of 3 GHz is observed. Based on relative intensity noise (RIN) measurements, the laser's relaxation frequency is confirmed to occur at 7.7 GHz for the same bias current condition. In Fig. 6(a), the phase being disturbed in the dip area, the α_H-factor is estimated to be about $+0.17$ outside this region. Such a

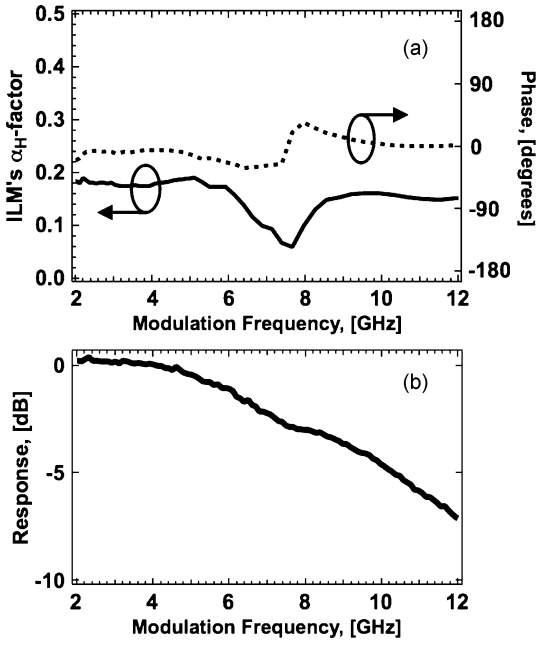

Fig. 6. (a) Measured α_H-factor amplitude (solid line) and phase (squared line) as a function of the modulation frequency for the ILM. (b) Corresponding AM response.

perturbation appears more pronounced on the chirp characteristic, as compared with the AM response on which this phenomenon could be less perceptible, as shown in Fig. 6(b).

3.4. Evaluation of the α_H-Factor's Experimental Accuracy

This section aims to evaluate the experimental accuracy related to the measurement of the α_H-factor (or to the $2\beta/m$ ratio) in the case of $f_m = 10$ GHz. This last value is considered because it corresponds to a realistic value used for the determination of the chirp parameter (see Section 3.1). Typically, the two main sources of uncertainties occurring in the determination of the α_H-factor are those related to the accuracy of the FSR of the MZ interferometer, as well as to the linearity of the electrooptics network analyzer. All other contributions can be neglected and have minor effects, as compared with the overall accuracy. For instance, the electrical frequency modulation f_m is known with an accuracy of 10^{-5}, while we can demonstrate that the locations around the points A and B have no effect, at the first order, on the signal measured by the network analyzer.

- Accuracy on the FSR
  In the Appendix, it is shown that the FSR is equal to 47.6 $\pm$ 0.2 GHz.
  Consequently, for $f_m = 10$ GHz, accuracy of the term $\tan(\pi f_m/\mathrm{FSR})$ occurring in (9a) and (17) does not exceed 0.7%.
- Nonlinearity of the electrooptics network analyzer
  First, let us note that in the case of the CPR and α_H-factor measurements, the network analyzer's calibration is not required since the correction factor vanishes through the ratio $|(M_+ - M_-)/(M_+ + M_-)|$, which occurs in the set of (9a), (10), and (17). Consequently, only the nonlinear behavior of the network analyzer has to be taken into account for the estimation of the experimental accuracy. Thus, by using a referenced optical attenuator, the deviation of the analyzer's linearity at 10 GHz and, in the optical power operating range at the input of the photo-detector, is found to be at most equal to 0.15 dB, which can lead to an error of 1.7% on the ratio $|M_+/M_-|$. In Table 1, the experimental accuracy of the α_H-factor (or of the $2\beta/m$ ratio) has been evaluated, taking into account both the nonlinearity of the analyzer, as well as the additional contribution of the FSR. Calculations are done for different values of the α_H-factor

TABLE 1

Experimental accuracy on the α_H-factor taking into account both the nonlinearity of the analyzer as well the additional contribution of the FSR. Calculations are done for different values of the α_H-factor and at $f_m = 10$ GHz

$\lvert\alpha_H\rvert$	Variation due to the nonlinearity (%)	Variation due to the FSR (%)	Total (%)
0.1	12.6	0.7	14
0.2	5.8	"	7
0.5	1.8	"	2.5
1.0	0.4	"	1.1
2.0	0.75	"	1.5
5.0	3.1	"	4.0
10.0	6.9	"	8.0
20.0	15.2	"	16.0

and at $f_m = 10$ GHz. Let us note that regarding the CPR [see (10)], the output power precision ($\pm 2\%$ in the best case [40]) has to be included in the accuracy calculations.

We also have to consider the assumption made in (7)

$$J_1\left(2\beta\sin\left(\frac{\pi f_m}{FSR}\right)\right) \approx \beta\sin\left(\frac{\pi f_m}{FSR}\right).$$

For instance, for $m = 10\%$ and $\alpha_H = 2$, the calculated deviation is 0.2% for $f_m = 10$ GHz but increases to 1.2% for $\alpha_H = 5$. However, let us stress that such a deviation remains negligible as long as $m \leq 5\%$.

4. Conclusion

In this paper, an optical discriminator based on a tunable MZ interferometer has been used to extract FM/AM ratio, as well as the α_H-factor for both laser diodes and EAM-based devices. As such a method allows the determination of both modulus and phase over a wide frequency span, more relevant information on the chirp can be extracted, as compared with the traditional techniques like the fiber transfer method, which only holds under the assumption that the chirp is not frequency-dependent. In case of DFB lasers, the proposed method also allows evaluation of the adiabatic chirp and the thermal effects. With regard to the EAM, the experimental results have been found to be in a very good agreement with those obtained from the fiber transfer. As discussed, the proposed technique is also much quicker, as compared with the fiber transfer one and can also be used to evaluate the influence of the optical feedback on the EAM's laser section. Finally, let us stress that the proposed experimental setup can also cover a wide range of operating wavelengths since only the couplers and the optical fibers are wavelength-sensitive and can easily be converted to a large-signal analysis configuration [31], leading to complementary results from those presented in this paper. As compared with other techniques, this method based on a tunable MZ interferometer requires no fitting parameters and, thus, is a reliable tool, which can be used for the characterization of high-speed properties of semiconductor diode lasers and EAMs.

Appendix

Determination of the Optimum Value of the FSR of the MZ Interferometer

Relationships obtained in Section 2 allow determination of the optimum value of the FSR. Indeed, the term $\tan(\pi f_m/FSR)$ occurring in (9a), (10), and (17) can be a source of uncertainty especially

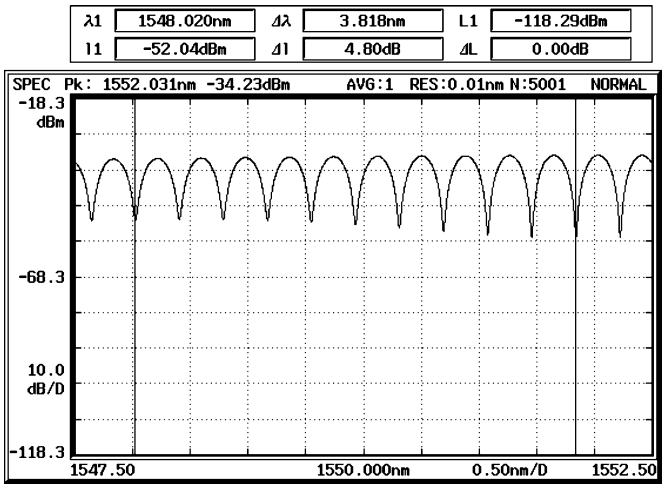

Fig. 7. Measurement of the transfer function of the MZ interferometer.

when the modulation frequency gets closer to half of the FSR (see Section 3.4). In our case, measurements are conducted up to 20 GHz (corresponding to the network analyzer bandwidth limit) so that the FSR of the interferometer has to be a bit greater than 40 GHz. As demonstrated in Section 2.2 for the laser case, the signals measured by the network analyzer can be expressed as follows (8):

$$M_{\pm} = \frac{P_0}{2} m \cos\left(\frac{\pi f_m}{FSR}\right) \exp(-j2\pi f_m \tau) \pm P_0 \frac{\Delta F}{f_m} \sin\left(\frac{\pi f_m}{FSR}\right) \exp j(-2\pi f_m \tau + \varphi) \tag{A1}$$

in which the parameter β has been replaced by its definition.

To simplify (A1), let us consider the case $FSR \gg f_m$. In that case, the following approximations can be made $\cos(\pi f_m/FSR) \approx 1$ and $\sin(\pi f_m/FSR) \approx \pi f_m/FSR$ such that (A1) becomes

$$M_{\pm} = \frac{P_0}{2} m \exp(-j2\pi f_m \tau) \pm P_0 \pi \frac{\Delta F}{FSR} \exp j(-2\pi f_m \tau + \varphi). \tag{A2}$$

When the FSR is too large, the second part of the right-hand side of (A2) becomes much weaker compared with the first part. Consequently, this situation could enhance the sensitivity to noise and to experimental evolution between measurements in M_+ and M_- (small decoupling effect, ...).

As a conclusion, to overcome such a problem, a 50-GHz value was targeted at the time that the interferometer was built. The interferometer transfer function is measured with a broadband optical source and an optical spectrum analyzer (OSA) to obtain the value of the FSR. In Fig. 7, the obtained value between the two vertical solid lines is equal to $\Delta\lambda = 3.818$ nm (ten times the FSR). A result as accurate as 47.6 ± 0.2 GHz is deduced for the FSR where ± 0.2 GHz takes into account both the accuracy of the OSA as well as the experimental resolution related to the position of the minima on the interferometer's characteristic.

Acknowledgment

The authors would like to thank D. Leclerc, who proposed to work on this subject, and J.-L. Beylat, H. Bissessur, T. Ducelier, J. Jacquet, C. Kazmierski, C. Smith, and B. Thedrez for fruitful discussions and encouragements.

References

[1] C. H. Henry, "Theory of the linewidth of semiconductor lasers," *IEEE J. Quantum Electron.*, vol. QE-18, no. 2, pp. 259–264, Feb. 1982.

[2] H. Su, L. Zhang, A. L. Gray, R. Wang, T. C. Newell, K. J. Malloy, and L. F. Lester, "Linewidth study of InAs-InGaAs quantum dot distributed feedback lasers," *IEEE Photon. Technol. Lett.*, vol. 16, no. 10, pp. 2206–2208, Oct. 2004.

[3] K. Petermann, *Laser Diode Modulation and Noise*. Norwell, MA: Kluwer, 1991.

[4] D. M. Kane and K. A. Shore, *Unlocking Dynamical Diversity*. Hoboken, NJ: Wiley, 2005.

[5] F. Grillot, N. A. Naderi, M. Pochet, C.-Y. Lin, and L. F. Lester, "Variation of the feedback sensitivity in a 1.55-μm InAs/InP quantum-dash Fabry–Perot semiconductor laser," *Appl. Phys. Lett.*, vol. 93, no. 19, p. 191 108, Nov. 2008.

[6] J. Marciante and G. P. Agrawal, "Nonlinear mechanisms of filamentation in broad-area semiconductor lasers," *IEEE J. Quantum Electron.*, vol. 32, no. 4, pp. 590–596, Apr. 1996.

[7] M. Osinski and J. Buus, "Linewidth broadening factor in semiconductor lasers—An overview," *IEEE J. Quantum Electron.*, vol. QE-23, no. 1, pp. 9–29, Jan. 1987.

[8] G. Giuliani, S. Donati, A. Villafranca, J. Lasobras, I. Garces, M. Chacinski, R. Schatz, C. Kouloumentas, D. Klonidis, I. Tomkos, P. Landais, R. Escorihuela, J. Rorison, J. Pozo, A. Fiore, P. Moreno, M. Rossetti, W. Elsiisser, J. Von Staden, G. Huyet, M. Saarinen, M. Pessa, P. Leinonen, V. Vilokkinen, M. Sciamanna, J. Danckaert, K. Panajotov, T. Fordell, A. Lindberg, J.-F. Hayau, J. Poette, P. Besnard, F. Grillot, M. Pereira, R. Nelander, A. Wacker, A. Tredicucci, and R. Green, "Round-robin measurements of linewidth enhancement factor of semiconductor lasers in COST 288 action," presented at the Conf. Lasers Electro-Optics (CLEO) Europe/Int. Quantum Electronics Conf. (IQEC), Munich, Germany, 2007, Paper CB9-2-WED.

[9] F. Grillot, B. Dagens, J. G. Provost, H. Su, and L. F. Lester, "Gain compression and above threshold linewidth enhancement factor in 1.3-μm InAs-GaAs quantum-dot lasers," *IEEE J. Quantum Electron.*, vol. 44, no. 10, pp. 946–951, Oct. 2008.

[10] B. W. Hakki and T. L. Paoli, "Gain spectra in GaAs double-heterostructure injection laser," *J. Appl. Phys.*, vol. 46, no. 3, pp. 1299–1306, Mar. 1975.

[11] I. D. Henning and J. V. Collins, "Measurements of the semiconductor laser linewidth broadening factor," *Electron. Lett.*, vol. 19, no. 22, pp. 927–929, Oct. 1983.

[12] G. P. Agrawal, "Effect of gain and index nonlinearities on single-mode dynamics in semiconductor lasers," *IEEE J. Quantum Electron.*, vol. 26, no. 11, pp. 1901–1909, Nov. 1990.

[13] Z. Toffano, A. Destrez, C. Birocheau, and L. Hassine, "New linewidth enhancement determination method in semiconductor lasers based on spectrum analysis above and below threshold," *Electron. Lett.*, vol. 28, no. 1, pp. 9–11, Jan. 1992.

[14] A. Villafranca, J. A. Lázaro, I. Salinas, and I. Garcés, "Measurement of the linewidth enhancement factor in DFB lasers using a high-resolution optical spectrum analyzer," *IEEE Photon. Technol. Lett.*, vol. 17, no. 11, pp. 2268–2270, Nov. 2005.

[15] A. Villafranca, A. Villafranca, G. Giuliani, and I. Garces, "Mode-resolved measurements of the linewidth enhancement factor of a Fabry–Perot laser," *IEEE Photon. Technol. Lett.*, vol. 21, no. 17, pp. 1256–1258, Sep. 2009.

[16] R. Hui, A. Mecozzi, A. D'Ottavi, and P. Spano, "Novel measurement technique of α-factor in DFB semiconductor lasers by injection locking," *Electron. Lett.*, vol. 26, no. 14, pp. 997–998, Jul. 1990.

[17] G. Liu, X. Jin, and S. L. Chuang, "Measurement of linewidth enhancement factor of semiconductor lasers using an injection-locking technique," *IEEE Photon. Technol. Lett.*, vol. 13, no. 5, pp. 430–432, May 2001.

[18] Y. Yu, G. Giuliani, and S. Donati, "Measurement of the linewidth enhancement factor of semiconductor lasers based on the optical feedback self-mixing effect," *IEEE Photon. Technol. Lett.*, vol. 16, no. 4, pp. 990–992, Apr. 2004.

[19] C. Palavicini, G. Campuzano, B. Thedrez, Y. Jaouen, and P. Gallion, "Analysis of optical-injected distributed feedback lasers using complex optical low-coherence reflectometry," *IEEE Photon. Technol. Lett.*, vol. 15, no. 12, pp. 1683–1685, Dec. 2003.

[20] C. Harder, K. Vahala, and A. Yariv, "Measurement of the linewidth enhancement factorα of semiconductor lasers," *Appl. Phys. Lett.*, vol. 42, no. 4, pp. 328–330, Feb. 1983.

[21] R. Schimpe, J. E. Bowers, and T. L. Koch, "Characterization of frequency response of 1.5-μm InGaAsP DFB laser diode and InGaAs PIN photodiode by heterodyne measurement technique," *Electron. Lett.*, vol. 22, no. 9, pp. 453–454, Apr. 1986.

[22] U. Kruger and K. Kruger, "Simultaneous measurement of the linewidth enhancement factorα, and FM and AM response of a semiconductor laser," *J. Lightw. Technol.*, vol. 13, no. 4, pp. 592–597, Apr. 1995.

[23] T. Zhang, N. H. Zhu, B. H. Zhang, and X. Zhang, "Measurement of chirp parameter and modulation index of a semiconductor laser based on optical spectrum analysis," *IEEE Photon. Technol. Lett.*, vol. 19, no. 4, pp. 227–229, Feb. 2007.

[24] F. Devaux, Y. Sorel, and J. F. Kerdiles, "Simple measurement of fiber dispersion and of chirp parameter of intensity modulated light emitter," *J. Lightw. Technol.*, vol. 11, no. 12, pp. 1937–1940, Dec. 1993.

[25] A. Royset, L. Bjerkan, D. Myhre, and L. Hafskjaer, "Use of dispersive optical fibre for characterisation of chirp in semiconductor lasers," *Electron. Lett.*, vol. 30, no. 9, pp. 710–712, Apr. 1994.

[26] R. C. Srinivasan and J. C. Cartledge, "On using fiber transfer functions to characterize laser chirp and fiber dispersion," *IEEE Photon. Technol. Lett.*, vol. 7, no. 11, pp. 1327–1329, Nov. 1995.

[27] H. Olesen and G. Jacobsen, "Phase delay between intensity and frequency modulation of a semiconductor laser (including a new measurement method)," in *Proc. ECOC*, 1982, pp. 291–295, Paper BIV-4.

[28] D. Welford and S. B. Alexander, "Magnitude and phase characteristics of frequency modulation in directly modulated GaAlAs semiconductor diode lasers," *J. Lightw. Technol.*, vol. LT-3, no. 5, pp. 1092–1099, Oct. 1985.

[29] E. Goobar, L. Gillner, R. Schatz, B. Broberg, S. Nilsson, and T. Tanbun-ek, "Measurement of a VPE-transported DFB laser with blue-shifted frequency modulation response from DC to 2 GHz," *Electron. Lett.*, vol. 24, no. 12, pp. 746–747, Jun. 1988.

[30] R. S. Vodhanel and S. Tsuji, "12 GHz FM bandwidth for a 1530 nm DFB laser," *Electron. Lett.*, vol. 24, no. 22, pp. 1359–1361, Oct. 1988.
[31] R. A. Saunders, J. P. King, and I. Hardcastle, "Wideband chirp measurement technique for high bit rate sources," *Electron. Lett.*, vol. 30, no. 16, pp. 1336–1338, Aug. 1994.
[32] R. Brenot, M. D. Manzanedo, J.-G. Provost, O. Legouezigou, F. Pommereau, F. Poingt, L. Legouezigou, E. Derouin, O. Drisse, B. Rousseau, F. Martin, F. Lelarge, and G. H. Duan, "Chirp reduction in quantum dot-like semiconductor optical amplifiers," presented at the Eur. Conf. Exh. Opt. Commun., Berlin, Germany, 2007, Paper we.08.6.6.
[33] W. V. Sorin, K. W. Chang, G. A. Conrad, and P. R. Herndday, "Frequency domain analysis of an optical FM discriminator," *J. Lightw. Technol.*, vol. 10, no. 6, pp. 787–793, Jun. 1992.
[34] T. L. Koch and J. E. Bowers, "Nature of wavelength chirping in directly modulated semiconductor lasers," *Electron. Lett.*, vol. 20, no. 25, pp. 1038–1040, Dec. 1984.
[35] L. Olofsson and T. G. Brown, "Frequency dependence of the chirp factor in 1.55 μm distributed feedback semiconductor lasers," *IEEE Photon. Technol. Lett.*, vol. 4, no. 7, pp. 688–691, Jul. 1992.
[36] L. A. Coldren and S. W. Corzine, *Diode Lasers and Photonic Integrated Circuits*. Hoboken, NJ: Wiley, 1995.
[37] F. Koyama and K. Iga, "Frequency chirping in external modulators," *J. Lightw. Technol.*, vol. 6, no. 1, pp. 87–93, Jan. 1988.
[38] P. Brosson and H. Bissessur, "Analytical expressions for the FM and AM responses of an integrated laser-modulator," *IEEE J. Sel. Topics Quantum Electron.*, vol. 2, no. 2, pp. 336–340, Jun. 1996.
[39] N. H. Zhu, G. H. Hou, H. P. Huang, G. Z. Xu, T. Zhang, Y. Liu, H. L. Zhu, L. J. Zhao, and W. Wang, "Electrical and optical coupling in an electroabsorption modulator integrated with a DFB laser," *IEEE J. Quantum Electron.*, vol. 43, no. 7, pp. 535–544, Jul. 2007.
[40] D. Derickson, *Fiber Optic Test and Measurement*. Englewood Cliffs, NJ: Prentice-Hall, 1998.